Non-destructive testing investigation of gaps in thin Glare laminates

Jakubczak, Patryk; Nardi, Davide; Bienas, Jaroslaw; Sinke, Jos

DOI
10.1080/10589759.2019.1684489

Publication date
2019

Document Version
Accepted author manuscript

Published in
Nondestructive testing and evaluation

Non-destructive testing investigation of gaps in thin Glare laminates

Patryk Jakubczak[1*], Davide Nardi[2], Jarosław Bieniaś [1], Jos Sinke[2]

[1] Department of Materials Engineering, Faculty of Mechanical Engineering, Lublin University of Technology, Nadbystrzycka 36, 20-618 Lublin, Poland.

[2] Department of Aerospace Structures and Materials, Faculty of Aerospace Engineering, Delft University of Technology, Kluyverweg 1, 2629 HS, Delft, The Netherlands.

* corresponding author: p.jakubczak@pollub.pl

Abstract

The manufacturing procedure of Fibre Metal Laminates (FMLs), such as Glare, consisting of alternating layers of pre-preg fibre and metal sheets is relatively complex, and defects can be introduced during manufacturing. The automation of the manufacturing steps is vital for future Glare production, and specific defects have to be considered. Among them, gaps between pre-preg plies represent a potential risk for the mechanical performances of the final laminate. In this paper/research, non-destructive testing (NDT) based on ultrasonic inspections are performed on Glare laminates with pre-preg gaps in order to extend and improve the current state of the art to different pre-preg gap widths, depths, and specimen lay-ups. Firstly, gaps were introduced in Glare specimens. Then, a conventional C-scan ultrasonic inspection is performed. In order to overcome the current limitations of a top or planar view of the laminates, the evaluation of the depth of the gaps in the laminates is performed by means of phased array pulse-echo ultrasonic testing (PAUT). Lastly, images of the laminate cross-section cut-outs have been collected in order to provide a meaningful evidence of the ultrasonic-based analysis. Results from different Glare lay-ups and gap widths and depths show the accuracy of the proposed investigation which is able to provide a detailed assessment of the gap occurrences also for very thin laminates, paving the way for portable and faster quality control strategies for future automated Glare manufacturing.

Kay words: Glare, NDT, Defects, Gaps, Phased Array Ultrasonic Testing..

1. Introduction

FMLs represent an available and effective material class for applications in primary aircraft structures. Metal layer thicknesses ranging from 0.2 to 0.4 mm represent the optimal values. Glare, a member of FMLs, is composed of aluminium 7475-T761 or 2024-T3 and unidirectional S2-glass fibres embedded with FM94 adhesive, with a nominal thickness of 0.127mm. The pre-preg is laid in different orientations between the aluminium alloy sheets (as shown in Figure 1), leading to different standard grades [1]. For instance, a Glare 3-2/1-0.3 refers to a laminate with 2 aluminium sheets of 0.3 mm of thickness, and 1 cross-ply (0/90) pre-preg composite. Laminates made of Glare are currently used on the sections of the fuselage of the Airbus A380.

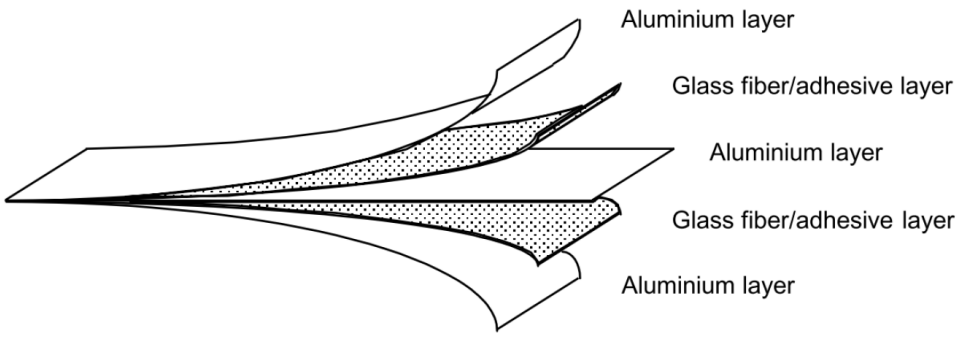

Fig. 1. Typical laminate lay-up for Glare [2].

The Glare superior behaviour in terms of fatigue crack initiation and growth, impact and fire resistance, and residual strength with respect to monolithic aluminium leads to weight and cost production savings [3-5]. The current production process is based on manual steps, such as aluminium sheets pre-treatment and bonding primer application, lay-up, NDE, and milling after the laminate curing [6].

To improve the production rate and to reduce the production cost, automated manufacturing of FMLs represents a significant goal for future applications in the aerospace field. One possible solution is to use automated tape laying process (ATP) for pre-preg roll in conjunction with picking-and-placing for the aluminium sheets [7,8].

As all the materials that are manufactured and used in structural components, also Glare is susceptible to defects or damage during the manufacturing and assembly stages, such as delaminations [1], inclusions [9], voids and porosity [1], disbonds [1,10], surface defects [9], fibre misalignment [11], and buckling [12], or during the operational life, like surface damage, penetration damage, matrix and aluminium cracks. Hence, a proper NDT routine is of utmost importance for a reliable Glare component quality control [13].

Various inspection methods have proven their effectiveness in the detection of different defects and damages in Glare structures. The most consolidated are based on ultrasonic C-scan inspections [9,14-18]. Ultrasonic inspections are based on differences in sonic transmission of different materials and reflection on interfaces in laminates. Ultrasonic waves (frequency $f > 50$ kHz) are transmitted through the laminate under inspection. Since the frequencies are so high, very short wavelengths are generated. This implies that very small discontinuities can be found because their size is approximately in the same order of magnitude as the wavelength. However, Glare poses a great challenge for ultrasonic-based NDT due to its anisotropic nature, the complex structure comprehending interlaminar doubler, spliced areas, etc., and the thickness of the laminate [19,20].

Among other well-known NDT techniques used in Glare it is worth mentioning ultrasonic Lamb wave propagation [21,22], eddy current testing [13,16], x-ray radiography [16], thermography [23], and shearography [24]. In addition to the different constraints inherited in each single methodology, the common drawback is related to the limitation during in-service operations.

In order to perform reliable in-service inspections, the use of multiple ultrasonic arrays, namely phased array pulse-echo ultrasonic test (PAUT), have seen a great increase for NDT purposes [25]. This method can perform inspections with a relatively small mobile unit requiring only one-side access to the material. The advantages also entail the flexibility that allows a particular array to perform a range of different inspections from a single location, and the rapid visualization of the inner structural component [25,26].

In order to enhance the application of PAUT for Glare components, this paper presents an improved NDT routine for the detection and the evaluation of pre-preg gaps in Glare laminates. The presence of pre-preg gaps, resulting due to fibre placement movement, tow width variation, or complexity of manufactured part [27], has proven to negatively affect the mechanical properties both for fully composite materials [8,28-33] and also for Glare laminates [15,34], and it will constitute a potential issue for the future automation of Glare manufacturing [7,35].

A previous work by Airbus [20] has shown the results of a phased array inspection in terms of the detection of the presence and of the depth of defects such as splices/gaps, and overlaps. However, a comprehensive analysis of the sensitivity of the methodology with respect to different Glare lay-ups and defect widths along with a validation with the results obtained from a consolidated routine such as the C-scan is missing.

The paper begins by presenting illustrations of the manufactured Glare specimens with pre-preg gaps. Then it briefly describes the adopted C-scan and PAUT methodologies and the related experimental results. The discussion then focuses on the analysis of the gaps performed by means of microscope images of the specimens cross-section.

Results show the effectiveness of the proposed PAUT approach for the detection of the width and the depth of gaps in different Glare lay-ups, along with future strategies for more reliable phased array inspections.

2. Materials and methods

Two square Glare laminates with different lay-ups and gaps of different widths have been considered for the current investigation. Table 1 summarizes the features of the adopted laminates.

Table 1. Details of the manufactured laminates with gaps.

Laminate ID	Glare features	Dimensions [mm]	N° gaps	Width of the gap [mm]	Position of the gap (ply)
1	3-2/1-0.3	200x200	3	2	0°
				6	
				10	
2	3-3/2-0.3	280x280	2	5	

Figure 2 and 3 show the sketches of the laminates highlighting the features and the gaps position.

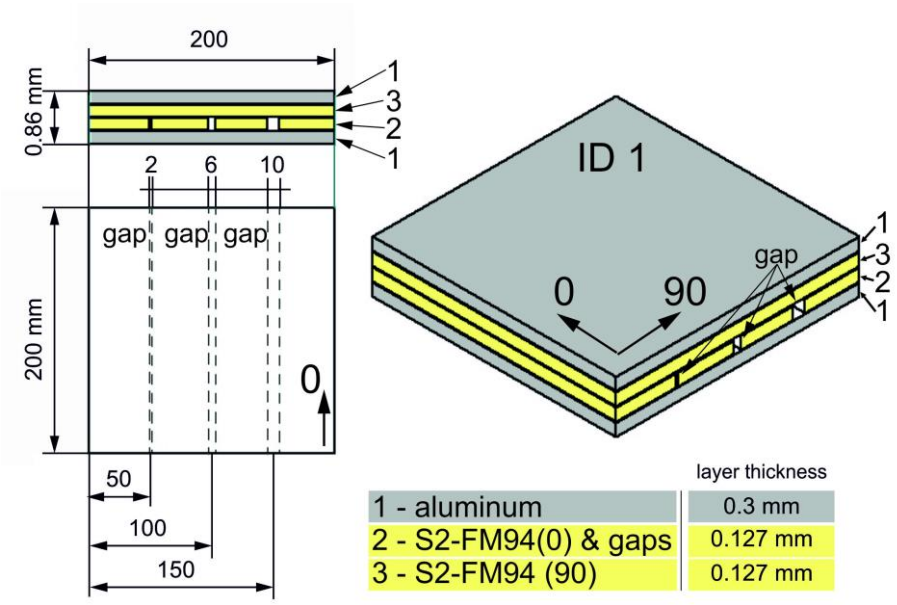

Fig. 2. Laminates ID 1 with gaps.

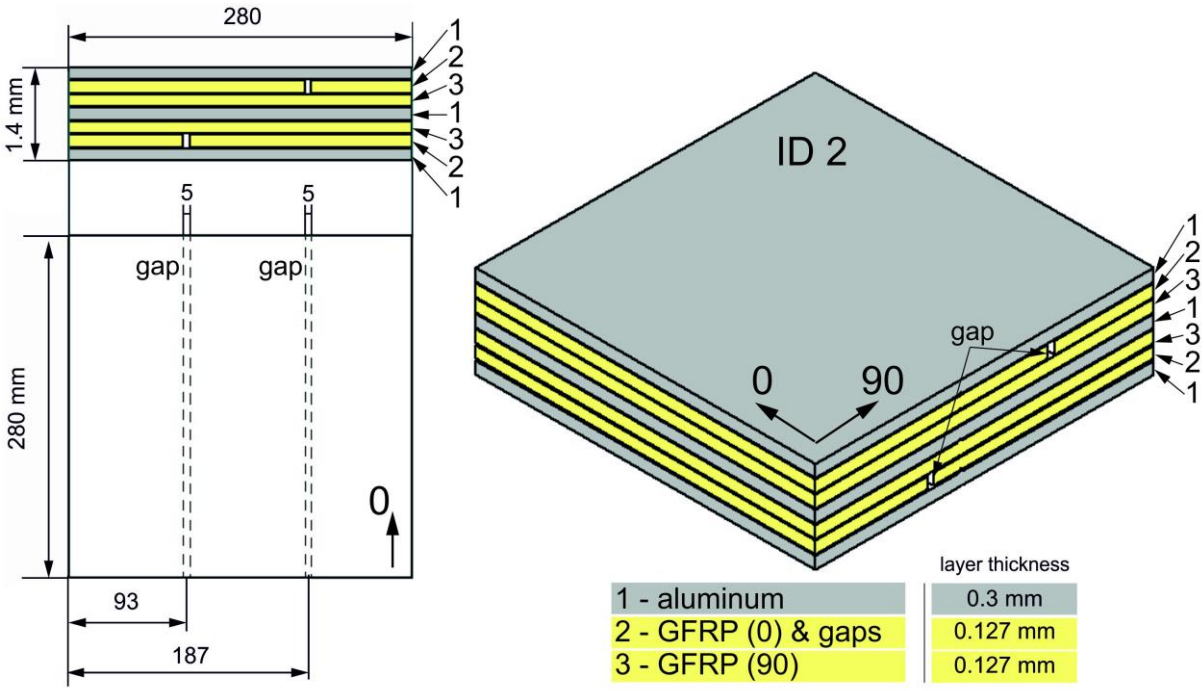

Fig. 3. Laminates ID 2 with gaps.

The laminates, have been subjected to ultrasonic non-destructive inspection in order to evaluate the effect of the presence of the manufactured gaps.

2.1. Non-destructive testing: C-scan

The adopted C-scan experimental set-up is shown in Figure 4, with the top and bottom squinters in the foreground. A schematic draw of the whole facility is reported in Figure 5.

Figure 4. C-scan top and bottom squirters.

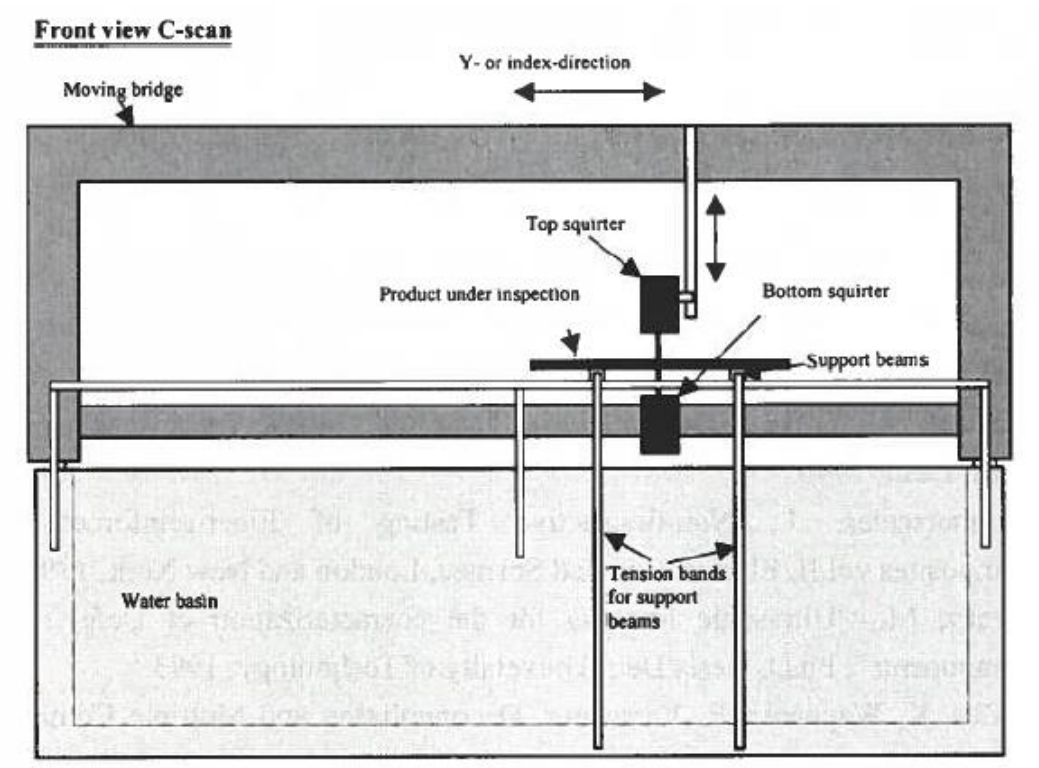

Figure 5. Sketch of the C-scan facility [9].

The adopted C-scan set-up is described as follow. The diameter of the ultrasound beam created by the transducer has been set equal to 8 mm, with a resolution of 1 mm (one pulse/mm) for the scanning pattern. The scanning rate has been set equal to 200 mm/s. The water squinters (water is used as a medium) have been placed at a distance of 20 cm, with the laminates placed between the squinters. The transducer frequency was set at 10 MHz since this represents the most sensitive frequency for general Glare quality assessment [9]. Table 2 summarizes the adopted C-scan setup.

Table 2. Data of C-Scan runs for the gaps investigation.

Width of the ultrasound beam [mm]	8
Scanning pattern resolution [mm]	1
Scanning rate [mm/s]	200
Transducer distance [cm]	20
Transducer frequency [MHz]	10

2.2. Non-destructive testing: Phased Array pulse – echo ultrasonic tests

The ultrasonic Phased Array pulse – echo Ultrasonic Tests (PAUT) was used with OmniScan MXU-M ultrasonic defectoscope (Olympus, Japan). Figure 6 shows the used phased array transducer features in detail. The phased array transducer had 64 active piezoelements operating at a frequency of 5 MHz (Olympus 5L64 A12, Japan). The head used the delay line with 10.15 μs wedge delay (the SA12-OL wedge line Olympus, Japan). Linear scan at 0º wave angle was used. Scanning size (active aperture) was 38.7 mm. The virtual aperture (VPA) was 8 piezoelements.

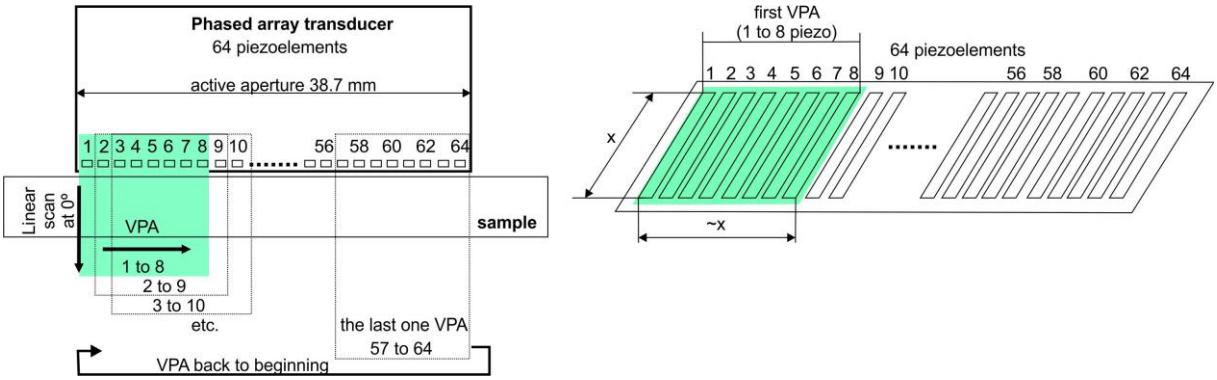

Fig. 6. The scheme of PAUT set up.

The A-scans were used for attenuation measuring (pulse-echo signals from one piezoelement). The B-scans (view from all piezoelements) were used to measure the total thickness of laminates and to measure the gap width and depth. Because of multi reflections of ultrasonic wave in fibre metal laminates caused by layers with different acoustic impedance (anisotropy of the material through the thickness) the measurements were provided in first pulse and echo of waves signals as well as in the second (derivative) reflection of wave. The measurements of the gaps depth as well as the panel thickness the velocity of the ultrasonic wave is required. The analytical method were used. In case of fibre metal laminates the wave velocity (v_{FML}) can be considered as a combination of the wave velocities in metal (v_M) and composite (v_C). Based on the simplification that the wave propagates in

different layers at different rates it is possible to compute the approximated value of the wave velocity using Equation 1.

$$v_{FML} = (MVF * v_M) + (1 - MVF) * v_C \quad (1)$$

where:
MVF is the Metal Volume Fraction [1]
v_M – is the ultrasonic wave velocity in aluminium. The value 6300 m/s were used (Olympus technical data sheet)
v_C – is the ultrasonic wave velocity in S2-FM94. The value 2900 m/s were used (Olympus technical data sheet).

Based on (1) the ultrasonic wave velocity for each specimen, the proper PAUT set up was evaluated and adopted.

3. Experimental investigation

3.1. C-scan

Figures 7 and 8 show the C-scan results of the Glare. A 6 dB value is used as a threshold level to evaluate the attenuation of flawed spots with respect to a reference flawless area. The palette colour scales on the left side of the figures are manually adjusted for a better representation of the results.

The red areas refer to the areas with higher attenuation (area where ultrasonic wave is disrupted by some changes inside the material), according to the palette on the left side. Note that the red areas at the sides of the laminates are due to the scanning pattern that goes outside the specimens dimensions and although they are visually as red as the gap area their dB attenuation value is higher (10 dB higher on average).

C-scan images reveal that (i) the gaps produce a course which for gaps of 5, 6, and 10 mm causes a higher attenuation at the edges of the course (red colour), while (ii) the area at the centre of the course has a lower attenuation compared to the edges. It is important to address the fact that only the right edge of such course presents a higher attenuation with respect to the left edge. Since this phenomenon occurs for both of the laminates the reason might be found in the adopted direction of the scanning pattern. The understanding of such occurrence is beyond the scope of the present section which aims at the detection of the gaps. However, in order to fully understand the reasons for areas of different attenuations, an optical investigation by means of microscope images of cross section cut-outs will be given in the following section 4.

For the gap of 2 mm instead, (iii) this effect does not manifest, and only a lower attenuation area with respect to the reference gapless areas is visible. For ID 2 laminate, the effect described in (i) is clearly visible for the gap on the left, and this is due to the different position of the two gaps along the thickness of the laminate.

In Table 3 the average attenuation values of gaps area are reported for the two laminates. Five random points in the highest attenuated areas are considered for the average computation.

Table 3. Average attenuation levels of the laminates.

	Average attenuation level [db]			
Laminates ID	Reference	Left Gap	Middle gap	Right gap
1	208.8 ± 5.4	221.4 ± 1.7	222.8 ± 1.5	180.0 ± 11.3
2	207.2 ± 0.4	221.0 ± 2.0	/	209.6 ± 3.7

From Figures 7 and 8 it is also possible to compute the width of the gaps. Such evaluation is performed by a dedicated ruler option available in the post processing tool. The values were taken measuring horizontally the start and the end of the red stripe.

Five random positions along the length of the gap have been selected for the average computation. The average values reported in Table 4 shows that there is a general trend for which the gap width is slightly overestimated.

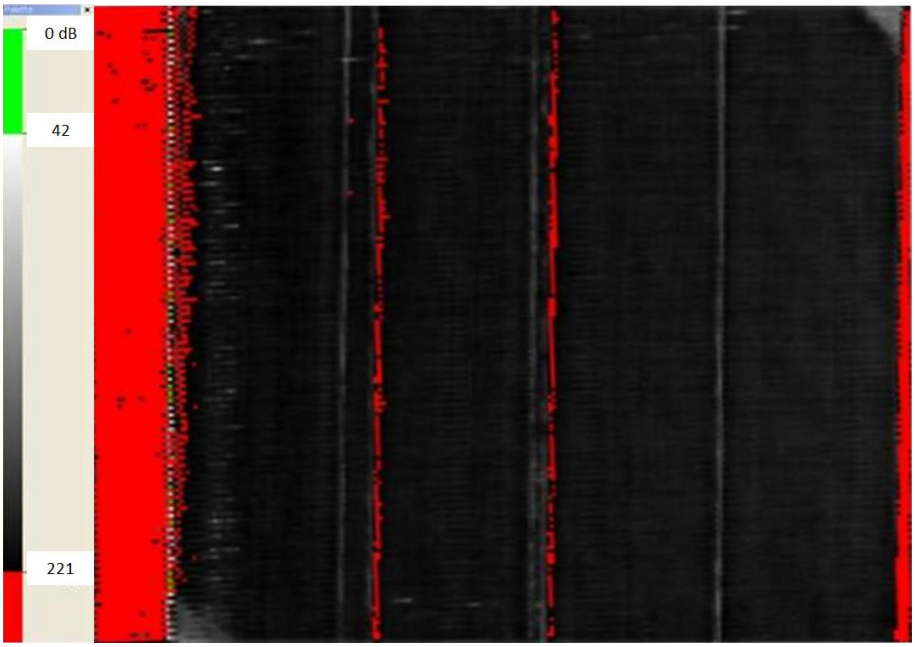

Fig. 7. C-scan image of ID 1 laminate.

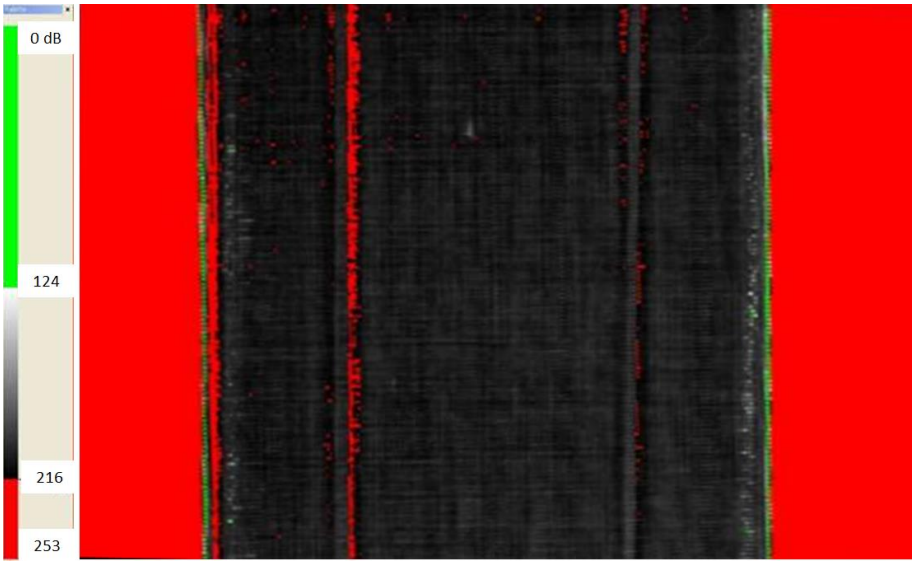

Fig. 8. C-scan image of ID 2 laminate.

Table 4. Average gap width of the laminates from C-scan images.

Laminates ID	Average Width [mm]					
	Left Gap		Middle gap		Right gap	
	Manufactured	Detected	Manufactured	Detected	Manufactured	Detected
1	10	9.8 ± 0.4	6	7.0 ± 0.7	2	2.4 ± 0.5
2	5	7.0 ± 0.7	/		5	6.6 ± 0.5

3.2. Phased Array pulse-echo ultrasonic tests

The results of PAUT ultrasonic scanning of ID 1 laminate are presented in Figure 9.

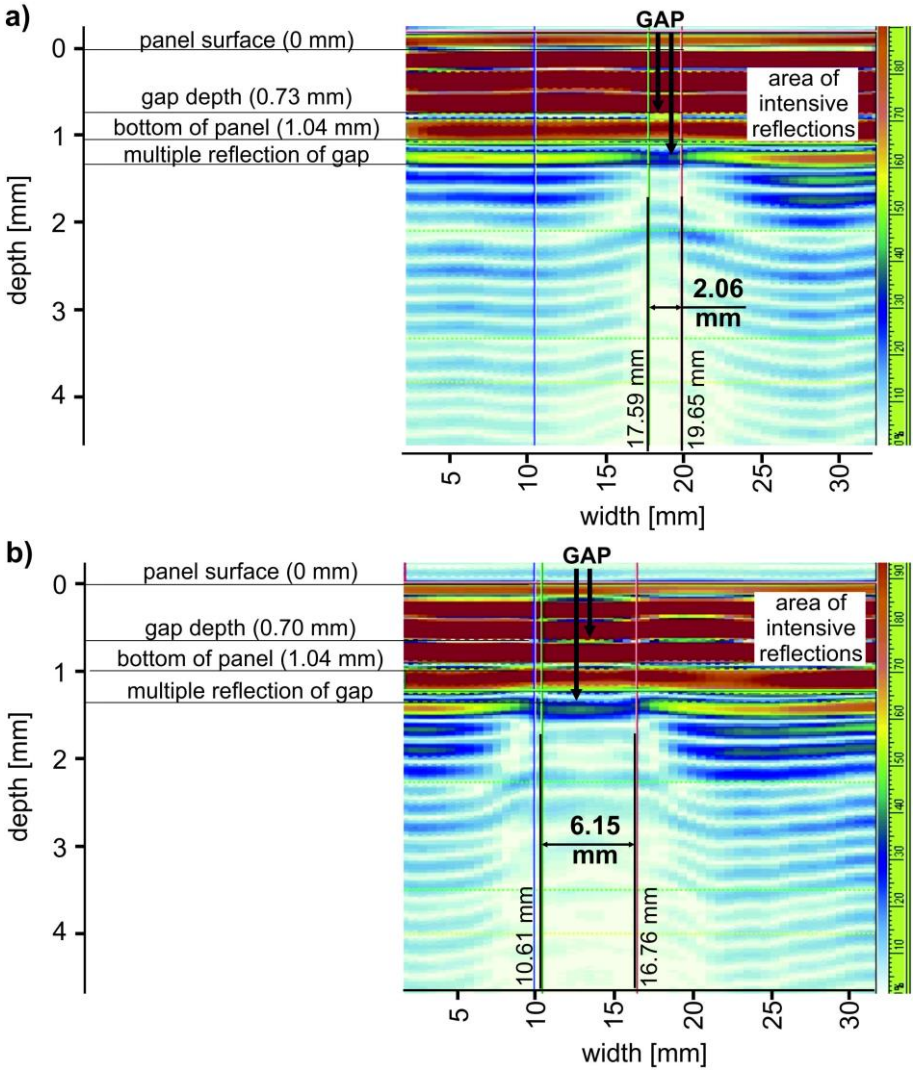

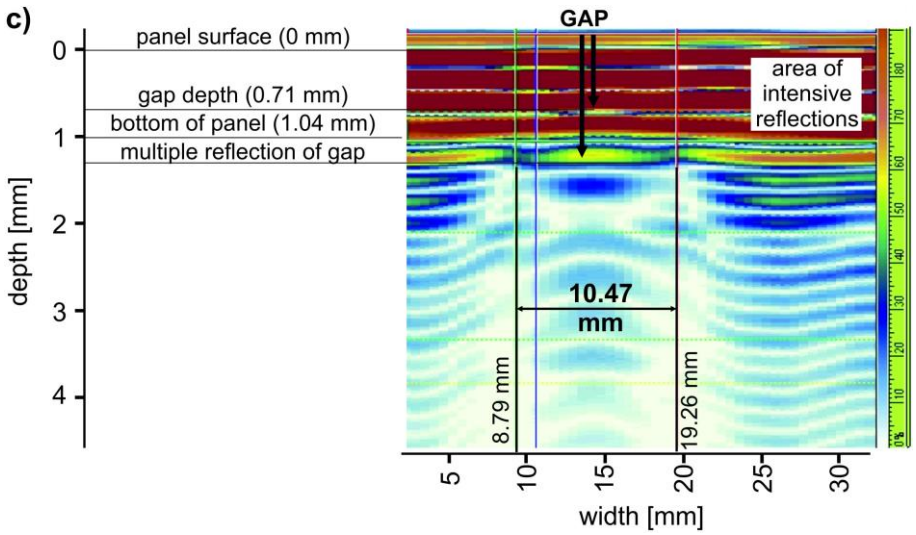

Fig. 9. Phased array B-scan test results of ID 1 laminate: manufactured gap width 2 mm (a), 6 mm (b) and 10 mm (c).

The PAUT results of ID 1 laminate present the cross sections (B-scans) of the laminate where area of intensive reflections of ultrasonic wave can be observed. Based on comparison of the cross section views through all the laminate areas, the regions with gaps were separated (see Fig. 9). Some anomalies in laminate layers can be noted especially in secondary reflections of UT wave. It can be observed that bottom lines are intermittent (Fig. 9) what corresponds to local disturbances of wave propagation in a laminate. Such anomalies as presented in Fig. 9 are synonymous with the presence of a defect inside the laminate. Because of small attenuations of the wave were noted (as reported in Table 5) the probability of gaps in such regions was assessed. Two arrows described as “gap” on figure 9 were drawn as a representation of first and second wave reflection because of the gap. The attenuation level of 20-25% is due to no empty spaces in material in gap region. E.g. in case of delamination, the inclusion of a foreign object such as foil or high porosity the attenuation of more than 50% is normal.

Secondly, based on physical parameters of the ultrasonic transducer (known width of active aperture in transducer) the width of each gap was determined (as presented in Table 5) as a width of a changed signal line because of higher attenuation (see. Fig. 9). According to wave signal recognition of the lower surface of Glare and the velocity of the ultrasonic wave propagation in the tested material the laminate total thickness was determined. Moreover, the depth of each gap was estimated. The depth should be considered as the top surface of the gap even if the gap has some thickness. However it should be considered that if the gap width is small, the detection becomes more difficult. Based on the B-scan analysis it can be assumed that the gap identification is possible as well as detailed dimensioning of the gaps.

The results of PAUT ultrasonic scanning of ID 2 laminate are presented in Figure 10.

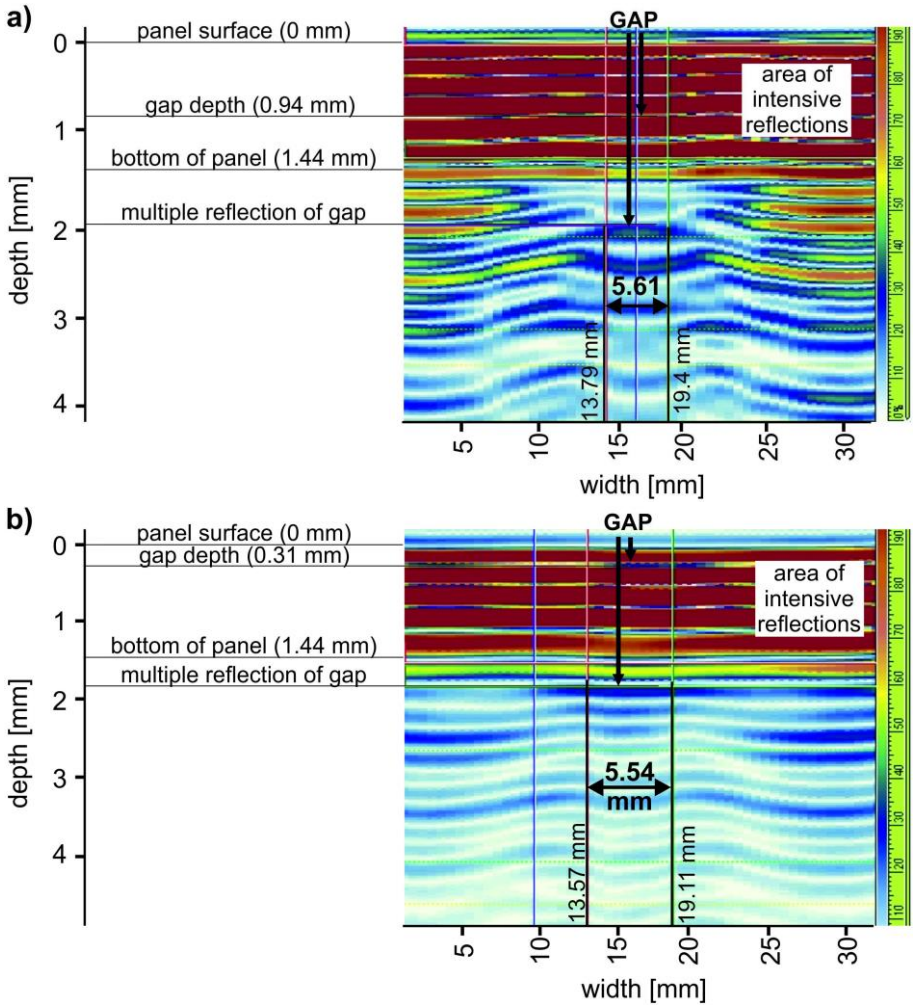

Fig. 10. Phased array B-scan tests results of ID 2 laminate. Bottom gap (a) and top gap (b).

In case of a more complex laminate (three aluminum layers and two composite layers) the total thickness of the specimen and the amount of interfaces with different acoustic impedance increase. These factors make the pulse–echo ultrasonic method less suitable for the observation of the defects. However, the 5 mm gap at the bottom of ID 2 laminate was easy to recognize (see. Fig. 10a) whilst the gap at the top was barely visible (see. Fig. 10b). The difficulties of top gap visualization is due to much lower attenuation in comparison with the bottom gap. The lower attenuation level in the case of laminate ID 2 can be the reason of the gap position near the transducer surface (close field). However, as in the case of ID 1 laminate the quantitative analysis of gaps in ID 2 laminate were possible. The gap widths and laminate thickness and each gap position through the thickness were determined. In Table 5 the overall results are presented.

Table 5. Phased Array pulse – echo ultrasonic tests results of GLARE panels.

Laminate	Total panel thickness (t) [mm]		Gap width (w) [mm]		Position (d) (through the thickness) [mm]		Attenuation [%]
	manufactured	measured	manufactured	measured	theoretical	measured	
1	0.86	1.04	2	2.06	0.42 < d < 0.55	0.73	24
			6	6.15	0.42 < d < 0.55	0.70	25
			10	10.47	0.42 < d < 0.55	0.71	22
2	1.40	1.44	5	5.61	0.98 < d < 1.11	0.94	35
			5	5.54	0.3 < d < 0.43	0.31	21

The quantitative analysis of gaps in tested laminates by using the PAUT technique shows good correlation between measurements and manufactured gap width and position, especially in case of ID 2 laminate. However, in case of ID 1 laminate (thinner laminate) some mismatch can be observed. In particular, 18% and 21% of mismatches for the thickness and for the depth values are obtained, respectively. The reason can be the found in the overlapping of the reflection signals from the lower surface with another surface such that a proper separation of the signal from the lower surface is possible. The result shows how thin laminates are sensitive for the quantitative evaluation of inner damages . The 21% mismatch is not significant when the laminate thickness is lower than 1 mm (the missed dimensions are small, no more than 0.2 mm) since the methodology can be still developed and the presented results can be still improved. In general, taking under consideration the laminate thickness and possibilities of gap depth assessment, it can be concluded that PAUT method allows enough approximate NDT of gaps in advanced level.

3.3. Signal to Noise Ratio analysis

Signal to Noise Ratio (SNR) is a measure used in science and engineering that compares the level of a desired signal to the level of background noise. SNR is defined as the ratio of signal power to the noise power, often expressed in decibels. A ratio higher than 1:1 (greater than 0 dB) indicates more signal than noise. The use of the **S**ignal to Noise Ratio index was delivered for the purpose of the gap comparison as a derivative of their features (Eg. 2) [36].

$$SNR\,[dB] = 10\log_{10}\frac{f(x,y)\_S}{f(x,y)\_B} \tag{2}$$

where:

f(x,y)_S – is the value of the signal in the gap area (signal value);

f(x,y)_B – is the value of the signal outside* the gap area (noise value).

*Outside the gap area refers to a random spot on laminate surface assuming the good quality of the laminate.

The SNR coefficient along with the gap position and the gap width were considered. The SNR coefficient were not used as a criterion of NDT method but as illustration of reaction of ultrasonic wave over the gap according gap width and depth. Figure 11 illustrates the dependences of SNR and ratio of gap position to total panel thickness (d/t) and SNR ratio vs measured gap width.

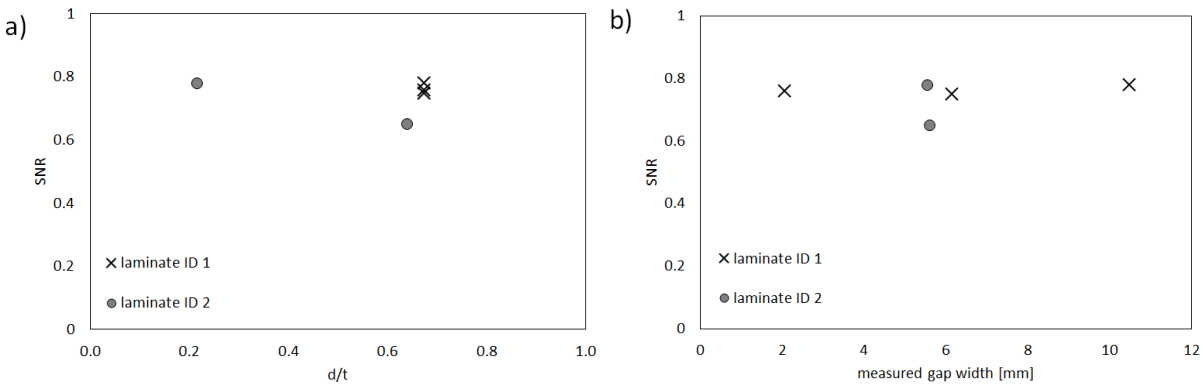

Fig. 11. SNR vs ratio of measured gap position to total thickness (a) and SNR ratio vs measured gap width.

In case of ID 1 laminate, (the gaps depths were constant) the SNR coefficient is nearly constant, even if the gaps width were different. In case of ID 2 laminate which have the same gaps width but different gaps depth some differences can be observed. SNR is about 20% lower in case of bottom gap because the higher value of SNR means worse detectability of gap. This is in agreement with the cross section analysis where the top gap was barely visible (as shown in Figure 10b). It can be assumed that gap depth can be a factor affecting the SNR coefficient value.
It was noted that the SNR coefficient is nearly the same for of all gaps in ID 1 laminate. Furthermore the SNR coefficient was different about 20% in case of ID 2 laminate even if the gaps width was the same. Based on the presented SNR relation to gap width (see Fig. 11b) it can be assumed that the width of gap has a limited influence to SNR coefficient.

3.4. Microstructure investigation

In order to understand the effect of the gap in the final cured laminate cross section cut-outs have been considered for gap microstructure investigation by means of a digital microscope.
Figure 12 shows two cut-outs from ID 1 laminate related to the gap on the right (2 mm).

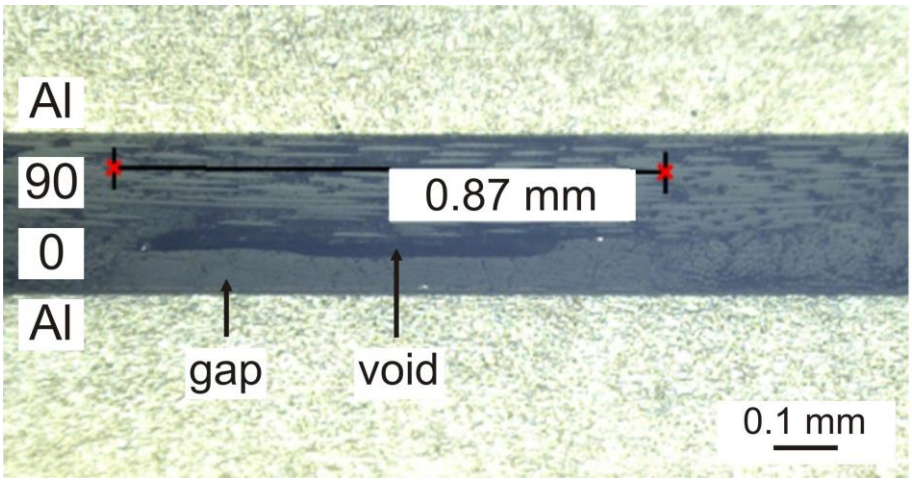

Fig. 12. Cut-outs of ID 1 laminate: right gap.

It can be seen from Figure 12 that the gap is filled with the epoxy from the adjacent pre-preg. However, a complete coverage of the gap area is not achieved and a void between the upper 90° fibres and the lower epoxy is clearly visible.

Figure 13 shows the cut-out from the gap in the middle (6 mm) of ID 1. What can be observed is that here the fibres from the top ply (90°) experience a pronounced waviness which occupies the gap that the epoxy from the adjacent pre-preg would not fill, as seen in Figure 12 for the gap of 2 mm. Therefore a higher gap width is accompanied by a higher fibre waviness. The same result is obtained from the gap on the left (10 mm) and also for the gaps of the ID 2 laminate.

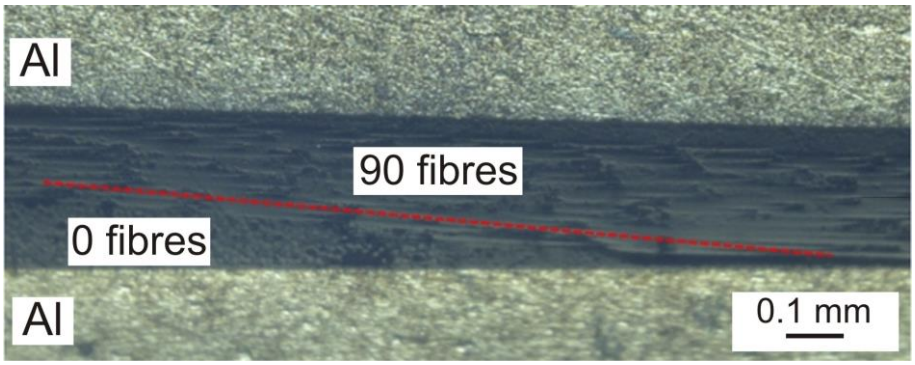

Fig. 11. Cut-out of ID 1 laminate: middle gap.

This waviness tendency explains also the reason for areas of different attenuation for the widest gaps (width > 2mm). Figure 14 shows the begin of the left gap in ID 1 (gap width of 10 mm). It is shown that the waviness effect is not able to fill the gap and therefore three areas appears: (1) the fibres just before the gap (flawless material with the dark grey colour in the C-scan images), (2) the void (flawed material with the red colour in the C-scan images on the edge of the gaps lane, and (3) the epoxy which has flown in the gap from the adjacent pre-preg (light grey colour in the C-scan images in middle of the gap lane).

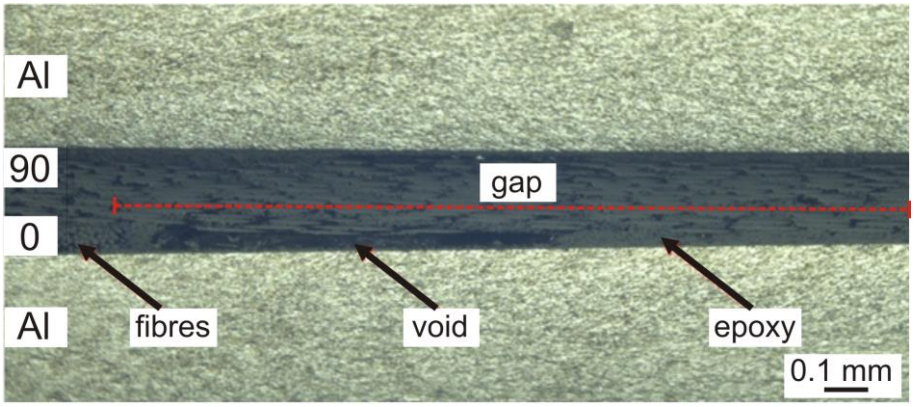

Fig. 14. Detail of the left gap in ID 1 laminate

From the cut-outs, the actual average width of the gaps in the laminate after the cure has been evaluated. The width of the gaps is measured considering the space left between the group of fibre on the left and on the right of the gap. The values are reported in Table 6.

Table 6. Average gap width of the laminates from microscope images

laminate ID	Average Width [mm]					
	Left Gap		Middle gap		Right gap	
	Manufactured	Actual	Manufactured	Actual	Manufactured	Actual
1	10	9.3 ± 0.4	6	5.0 ± 0.1	2	1.0 ± 0.1
2	5	5.3 ± 0.2	/		5	4.2 ± 0.1

Results show that there is a general trend in which the gap width reduces during the cure cycle of the laminate. Only for the left gap from ID 2, the average value is higher than the intended manufactured width. The most probable reason is that during the manufacturing the gap width has been wrongly made higher. However, the results show that the gap width that can be estimated from the C-scan images (see Table 4) is on average higher than the actual one.

The gap dimensions summary for NDT methods presented in Table 7 shows satisfactory correlation between the NDT measurements and the real values.

Table 7. Summary of the gap width detection.

Laminate	Average Width [mm]			
	Manufactured	C-scan	PAUT	Measured
3-2/1-0.3 (ID1)	2	2.4 ± 0.5	2.06	1.0 ± 0.1
	6	7.0 ± 0.7	6.15	5.0 ± 0.1
	10	9.8 ± 0.4	10.47	9.3 ± 0.4
3-3/2-0.3 (ID2)	5	7.0 ± 0.7	5.61	5.3 ± 0.2
	5	6.6 ± 0.5	5.54	4.2 ± 0.1

As it can be observed the PAUT as well as C-scan methods might slightly overestimate the actual gap width. The above can be connected with the diffraction phenomena of ultrasonic waves on the edges of gaps. However results show the reliability of the refined PAUT inspection for the through-the-thickness gap position detection even for very thin laminates, paving the way for fast and successfully NDT for future automated manufactured Glare laminates.

4. Conclusions

Glare represents an effective material for application in primary aircraft structures. Currently, the development of new automated manufacturing methods can lead to additional problems in Glare quality such as gaps and/or overlaps in internal composite layers. This is the reason why non-destructive inspection methods of Glare should be still improving in order to evaluate more accurate details about the presence of the defects.

The work presented a NDT routine of Glare specimens based on ultrasonic inspection. Consolidated C-scan and PAUT techniques have been considered for the detection of pre-preg gaps in Glare laminates.

However, the use of PAUT is extended to perform a detailed analysis of the defects in terms of detection, extension and depth estimation of the gaps. It was observed that the cross section visualization based on B-scan technique is promising for gaps with different widths and depths even in thin laminates as well as in complex FMLs such as 3/2 or 4/3 etc. Nonetheless, in order to make a correlation between the gap depth and the ply at which the gap occurs additional strategy can be developed in the future based on specially designed reference laminates with gaps.

5. Acknowledgement

This paper resulted as a collaboration between Delft University of Technology and Lublin University of Technology. The research was carried out under project number T11.6.14523 in the framework of the Research Program of the Materials innovation institute (M2i) (www.m2i.nl) supported by the Dutch government and Fokker Aerostructures, and in the framework of the project Lublin University of Technology-Regional Excellence Initiative, funded by the Polish Ministry of Science and Higher Education (contract no. 030/RID/2018/19).

6. References

1. Vlot A, Gunnink JW. Fibre Metal Laminates an introduction. Kluwer Academic Publishers 2001.
2. Beumler T. Flying GLARE. Ph.D. dissertation, Delft University of Technology 2004.
3. Alderliesten R, Homan JJ. Fatigue and damage tolerance issues of Glare in aircraft structures. Int J Fatigue 2006;28:1116-1123.
4. Roebroeks G.H.J.J. Fibre-metal laminates. Recent developments and applications. Int J Fatigue 1994;16(1):33-42
5. Bienias, J., Jakubczak, P. Impact damage growth in carbon fibre aluminium laminates. Compos Struct 2017;172:147-154
6. C van Hengel. Design for Value of FML Components: Example fuselage panels. Aeromat 2016.
7. Apmann H., Busse M., Du J.Y., Kohnke P. Automated Manufacture of Fibre Metal Laminates to Achieve High Rate of Production. Lightweight Design 2017;10:28-33.
8. Perner M., Algermissen S., Keimer R., Monner H.P.. Avoiding defects in manufacturing processes: A review for automated CFRP production. Robot Cim-Int Manuf 2016;38:82-92.
9. Coenen R.A.M. Design of a Quality Assurance System for Structural Laminates. Ph.D. dissertation, Delft University of Technology, 1998.
10. Nagy PB. Ultrasonic detection of kissing bonds at adhesive interfaces. J Adhesion Sci Technol 1991;5(8):619-630.
11. Yurgartis SW. Measurement of Small Angle Fiber Misalignments in Continuous Fiber Composites. Compos Sci Technol 1987;30:279-293.
12. Sinke J. Manufacturing of GLARE Parts and Structures. App Compos Mat 2003;10(4-5):293-305.
13. Sinke J. Some Inspection Methods for Quality Control and In-service Inspection of GLARE. Appl Compos Mater 2003;10:277-291.
14. Moriniere FD, Alderliesten RC, Tooski MY, Benedictus R. Damage evolution in GLARE fibre-metal laminate under repeated low-velocity impact tests. Central European Journal of Engineering 2012;2(4):603-611.
15. Nardi D., Abouhamzeh M., Leonard R., Sinke J. Detection and Evaluation of Pre-Preg Gaps and Overlaps in Glare Laminates. Appl Compos Mater 2018;25(6):1491-1507.
16. Fahr A, Chapman CE, Laliberte JF, Forsyth DS, Poon C. Nondestructive Evaluation Methods for Damage Assessment in Fiber-Metal Laminates. Polymer Composites 2000;21(4):568-575.
17. Bienias J, Jakubczak P, Majerski K, Ostapiuk M, Surowska B. Methods of ultrasonic testing, as an effective way of estimating durability and diagnosing operational capability of composite laminates used in aerospace industry. Eksploat Niezawodn 2013;15(3):284–289.

18. Czechowski, L., Gliszczyński, A., Bieniaś, J., Jakubczak, P., Majerski, K. Failure of GFRP channel section beams subjected to bending - Numerical and experimental investigations. Compos Part B-Eng 2017;111:112-123.
19. Mania R.J., Kolakowski Z., Bienias J., Jakubczak P., Majerski K. Comparative study of FML profiles buckling and postbuckling behaviour under axial loading. Compos Struct 2015;134:216-225.
20. Bisle W., Meier T., Mueller S., Rueckert S. In-Service Inspection Concept for GLARE - An Example for the Use of New UT Array Inspection System. 9th European Conference on NDT, Berlin, Germany, 2006.
21. Demcenko A, Zukauskas E, Kazys R, Voleisis A. Interaction of the A_0 Lamb Wave Mode With a De-Lamination Type Defect in GLARE3-3/2 Composite Material. Acta Acustica united with Acustica 2006;92:540-548.
22. Rosalie SC, Vaughan M, Bremner A, Chiu WK. Variation in the group velocity of Lamb waves as a tool for the detection of delamination in GLARE aluminium plate-like structures. Compos Struct 2004;66:77-86.
23. Ibarra-Castanedo C, Avdelidis NP, Grinzato EG, Bison PG, Marinetti S. Delamination detection and impact damage assessment of GLARE by active thermography. International Journal of Materials and Product Technology 2011;41.
24. Steinchen W, Yang L, Kupfer G, Mackel P. Non-destructive testing of aerospace composite materials using digital shearography. Proceedings of the Institution of Mechanical Engineers, Part G: Journal of Aerospace Engineering 1998;212:21-30.
25. Drinkwater B.W., Wilcox P.D. Ultrasonic arrays for non-destructive evaluation: A review. NDT&E 2006;39(7):525-541.
26. Felice M.V., Velichko A., Wilcox P.D. Accurate depth measurement of small surface-breaking cracks using an ultrasonic array post-processing technique. NDT&E Int 2014;68:105-112.
27. Elsherbini Y.M., Hoa S.V. Experimental and numerical investigation of the effect of gaps on fatigue behaviour of unidirectional carbon/epoxy automated fiber placement laminates. J Compos Mater 2017;51(6):759-772.
28. Sawicki A., Minguet P. The effect of intraply overlaps and gaps upon the compression strength of composite laminate. 39th AIAA structural, dynamics, & materials conference. Lomg Beach, CA, 744-754, 1998.
29. Croft K., Lessard L., Pasini D., Hojjati M., Chen J., Yousefpour A. Experimental study of the effect of automated fiber placement induced defects on performance of composite laminates. Compos Part A-Appl S 2011;42(5):484-491.
30. Falco O., Mayugo J., Lopes C.S., Gascons N., Costa J. Variable-stiffness composite panels: Defect tolerance under in-plane tensile loading. Compos Part A-Appl S 2014;63:21-31.
31. Fayazbakhsh K., Arian N.M., Paini D., Lessard L.. The effect of gaps and overlaps on the in-plane stiffness and buckling load of variable stiffness laminates made by automated fiber placement. Proceedings of 15th European Conference on Composite Materials, Venice, Italy, 2012.
32. Li X., Hallet S.R., Wisnom M.R. Modelling the effect of gaps and overlaps in automated fibre placement (AFP)-manufactured laminates. Sci Eng Compos Mater 2015;22(2):115-129.
33. Wang E.L., Gutowski T.G. Laps and gaps in thermoplastic composite processing. Composite Manufacturing 1991;2(2):69-78.
34. Abouhamzeh M, Nardi D, Leonard R, Sinke J. Effect of prepreg gaps and overlpas on mechanical properties of fibre metal laminates. Composites Part A: Applied Science and Manufacturing 2018;114:258-268.
35. Ucan H, Apmann H, Grassl G, Krombholz C, Fortkamp K, Nieberl D, Schmick F, Nguyen C, Akin D. Production technologies for lightweight structures made from fibre-metal laminates in aircraft fuselages. CEAS Aeronautical Journal 2018;9:1-11.

36. Bienias J., Jakubczak P., Surowska B., Dragan K., Low-energy impact behaviour and damage characterization of carbon fibre reinforced polymer and aluminium hybrid laminates, Arch Civ Mech Eng 2015;15(4):925-932.